

Short Communication

Temperature-dependent Degradation of the Copper Current Collectors in Lithium Ion Batteries Electrolyte

Yuhang Zhao^{1,#}, Ruicheng Fan^{1,#}, Shuwei Dai², Yunlei Lv², Yanjie Ren²,
Yifan Li¹, Yongwang Wang^{1,*}, Jian Chen^{2,*}

¹ Research center of ShenHua Zhunneng Comprehensive Resource Development Co. Ltd , Ordos 010300, China

² Key Laboratory of Energy Efficiency and Clean Utilization, Education Department of Hunan Province, Changsha University of Science & Technology, Changsha, Hunan 410114, China

#Yuhang Zhao and Ruicheng Fan contributed equally to this work

*E-mail: zgrwyw@126.com, chenjian5130@163.com

Received: 6 December 2020 / Accepted: 29 January 2021 / Published: 28 February 2021

Copper is usually used as a current collector in lithium ion batteries. Its stability is highly important in the performance of cell. In this paper, temperature dependent degradation of copper current collector was investigated at -20°C, 25°C and 50°C by electrochemical measurements. Scanning electron microscopy (SEM), X-ray diffraction (XRD) and energy dispersive spectroscopy (EDS) were used to analyze the microstructures of corroded copper. At -20°C and 25°C, obvious pitting corrosion occurs on the copper due to the self-catalyst of residual water. However, at 50°C, a loose layer containing a certain amount of LiF forms on the surface of the copper and no pitting hole is observed due to the exhaustion of the aggressive fluoride ions and the residual water.

Keywords: Lithium ion batteries; Copper current collector; Electrolyte; Temperature; Corrosion

1. INTRODUCTION

In 1972, the concept of rechargeable lithium rocking chair batteries was proposed by Armand[1]. In recent years, lithium ion batteries have gradually been used in many portable electronic devices, electric cars, laptops and military fields[2-5]. Typically, lithium ion batteries exhibit excellent performances under ambient conditions. However, with the increasing of the demand of consumers, more electric vehicles used in both colder regions and hot desert conditions, which requires the working temperatures of battery systems between -40°C to 60°C. Usually, for lithium ions batteries, the usable

capacity decreases and internal resistance increases at elevated temperatures or subzero temperatures during cycling and storage[6]. Specifically, at an elevated temperature, the spontaneous decomposition of the liquid electrolytes causes a lapse in the batteries' operation[7-8]. At subzero temperatures, the performance of lithium ion batteries degrades due to the low electrolyte conductivity[9], the reduced charge transfer kinetics[10,11], the increase in the solid electrolyte interphase resistance[12,13], and the slow solid-state lithium diffusivity[14,15]. Besides organic electrolyte, the effects of temperatures on the multiple anodic materials, such as $\text{Li}_{3.9}\text{Cr}_{0.3}\text{Ti}_{4.8}\text{O}_{12}$ and CuBi_2O_4 , have been evaluated[16,17]. Moreover, some references have reported the influence of the separator and additive on the cycling performance of the lithium ion battery in extreme environments[18,19].

The collector is a critical component of lithium ion batteries and its stability influences the cycling stability of lithium ions batteries[20]. It has been demonstrated that the collectors usually suffer corrosion at the ambient temperature of lithium ion batteries[21-22]. It is a common of view that the different corrosion mechanisms may be favored when the electrolyte is changed. Meanwhile, the conductivity of the electrolyte also affects the ohmic drop in potential between the anodic and cathodic reaction sites in situations such as pitting corrosion[23]. Thus, both the decomposition of electrolyte at an elevated temperature and the conductivity decrease of electrolyte at subzero in lithium ion battery would cause the different corrosion processes of copper foil collector. Until now, no reports concern about the corrosion behavior of copper foil collector in lithium ions batteries electrolyte at extreme conditions.

In this paper, the corrosion performance of copper in lithium ion batteries electrolyte at different temperatures have been investigated by electrochemical methods aiming to evaluate the chemical stability of copper foil collector at the extreme working conditions.

2. EXPERIMENTAL

Commercial T1 copper (99.95% purity) was chosen as raw material. The specimens with the size of 10 mm*5mm*5 mm were cut from the bulk. All of the experimental measurements were conducted in an electrolyte containing 1 mol/L LiPF_6 in a mixture of dimethyl carbonate (DMC), ethylene carbonate (EC) and ethyl methyl carbonate (EMC) (1:1:1) at -20°C , 25°C and 50°C , the residual water content of electrolyte was about 20 ppm. The containers for the organic electrolyte of lithium ions batteries were the polytetrafluoroethylene beakers and they were sealed by the rubber covers with a proper size to avoid oxygen ingress. In a glove box, the electrolyte of lithium batteries was poured into the beaker. Furthermore, a sealing tape was wrapped along the interface of the beak and the rubber cover to ensure the setup was well sealed.

All of the electrochemical measurements were conducted with a conventional three-electrode system with a copper sheet as the counter-electrode and a silver sheet as the reference electrode. The copper specimens, connected with copper wires by welding, were coated with epoxy resin with the exposed area 50mm^2 , and then were polished successively with 2000 emery paper, cleaned in distilled water and degreased in acetone, which are used as working electrode in the electrochemical experiments.

Electrochemical impedance spectroscopy (EIS) tests were conducted with a Zahner (Zennum) Potentiostat/Galvanostat in lithium ion batteries electrolyte. The electrochemical impedance measurement range was selected in the range of 0.01 Hz–100 kHz, with an amplitude of 10 mV for the input sine wave voltage. Potentiodynamic polarization was performed at a potential scanning rate of 60 mV·min⁻¹ from -250mV versus open circuit potential. For reproducibility, three specimens were used in the three distinct reproduced measurements.

The corroded samples were cleaned with de-ionized water and dried after corrosion testing. The surface morphologies of the specimens after the immersion tests were examined by a scanning electron microscopy (SEM) system (Quanta FEG 250, America). Analyses of the corrosion products and elemental compositions were examined by energy dispersive spectroscopy (EDS). The constituent phases of the particular corrosion products were identified through X-ray diffraction (XRD) analysis (Bruker D8 advance, Germany).

3. RESULTS AND DISCUSSION

3.1 Characteristic of the surface morphology

Figure 1 shows the surface morphologies of the copper sheets after immersion in the electrolyte at different temperatures. The high magnitude images of the red dashed loops in Figure 1 a and c are labeled as 1, 3 and 4. Figure 2 shows the corresponding EDS in the zone of 1, 2 and 3 and XRD analysis of the zone 4. A certain number of pits with a diameter of approximately 2 μ m on the surface of the copper after immersion in electrolyte at -20°C for 720h (as shown in Figure 1a). C, O, F and P can be detected in the pitting holes, indicating that corrosion products are mainly composed of copper oxides and copper fluorides. For the copper corroded in the electrolyte at 25°C, as shown in Figure 1b, some enlarged pitting holes and micro-cracks can be observed in the corrosion product layer, which is consistent with that reported by Shu[21]. The elemental composition in the pitting holes is similar to that corroded at -20°C.

However, when the temperature of electrolyte was elevated to 50°C, the corroded copper was partly covered by a loose corrosion product film. The corresponding XRD pattern of the products (as shown in Figure 2) shows that all the diffraction peaks can be indexed to LiF. Meanwhile, it could be observed that some tiny particles distribute on the blank zone, according to its high magnitude image as shown in Figure 1. Interestingly, the pit holes are not visible on the specimens corroded at 50°C. That is, copper immersed in the electrolyte at 50°C suffers a different corrosion process. The specific corrosion mechanisms will be elaborated in the following sections.

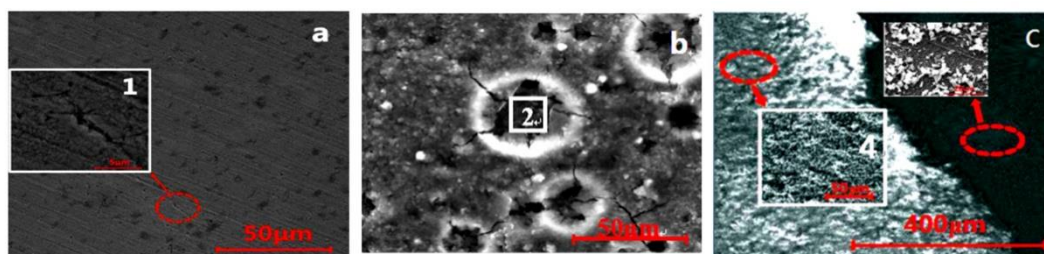


Figure 1. Surface morphologies of copper immersed in the electrolyte at (a)-20°C, (b) 25°C [21] and (c) 50°C for 720 h

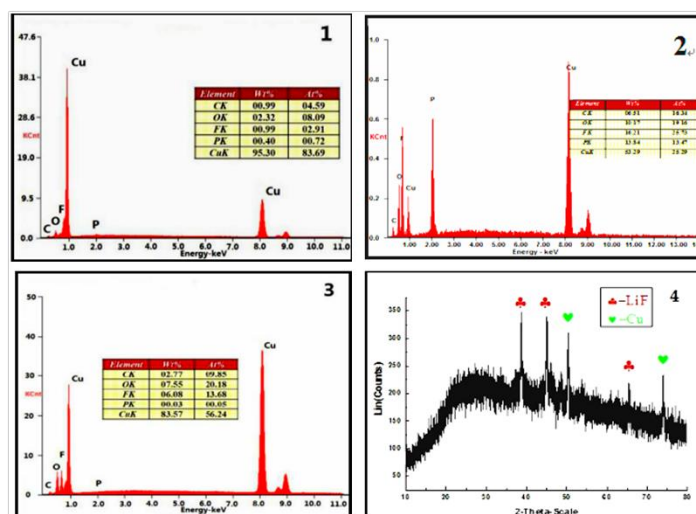


Figure 2. EDS analysis of copper immersed in the electrolyte (1) -20°C (2) 25°C[21] (3) 50°C (4) XRD analysis

3.2 Corrosion behavior of copper in lithium ion batteries electrolyte at different temperatures

3.2.1 Potentiodynamic polarisation curves

The potentiodynamic curves for copper after being immersed for 3 h at -20°C, 25°C and 50°C are shown in Figure 3. The copper specimens suffer from active dissolution in the electrolyte at free corrosion potential at all temperatures. The corrosion potential is 43mV, -97mV and 5mV at -20°C, 25°C and 50°C, respectively. The corrosion potential at -20°C is significantly higher than that at 25 °C, which is explainable according to Nernst equation. The higher potential value at 50°C is related to the composition variation of electrolyte during corrosion at an elevated temperature, which can be proved by the visible expansion of rubber cover for sealing. The analysis about that will be presented in the latter section. The corrosion current densities of samples corroded in electrolyte for 3 h at -20°C, 25°C and 50°C are 0.072 $\mu\text{A}\cdot\text{cm}^{-2}$, 0.107 $\mu\text{A}\cdot\text{cm}^{-2}$ and 6.91 $\mu\text{A}\cdot\text{cm}^{-2}$, respectively. According to Arrhenius equation, an elevated temperature caused a higher reaction rate constant during the electrochemical corrosion processes, as well as an increasing corrosion current density[24]. On the other hand, the variation of composition of electrolyte may promote the corrosion of copper.

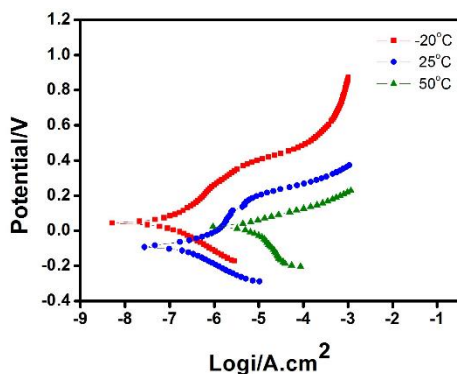


Figure 3. Potentiodynamic curves of copper after being immersed in the electrolyte for 3 h at different temperatures

3.2.2 Electrochemical impedance spectroscopy

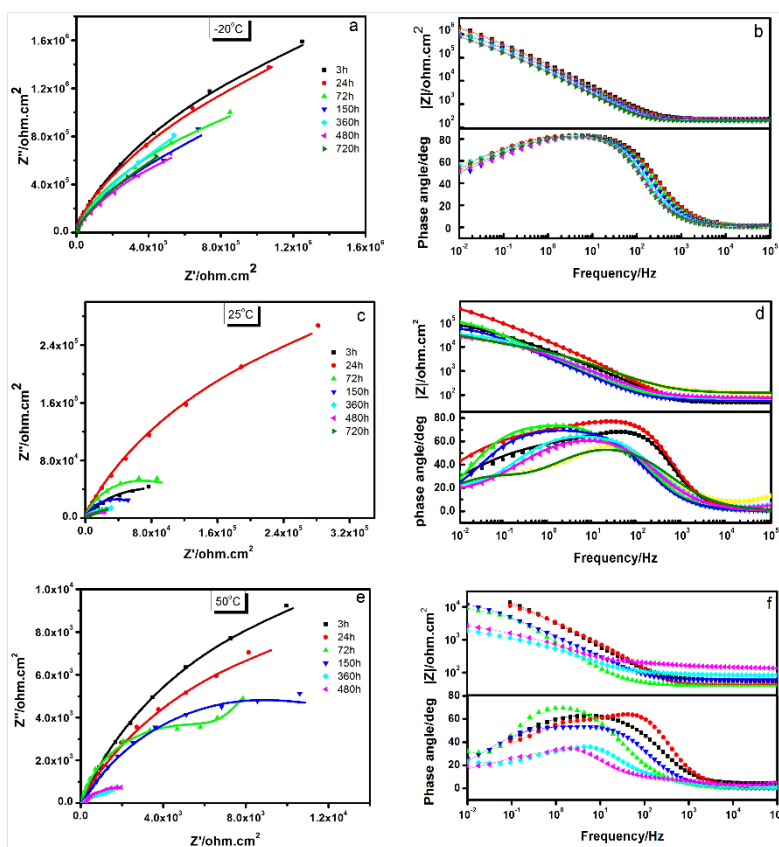


Figure 4. Nyquist and Bode plots for the copper in electrolyte at (a, b) -20°C (c, d) 25°C (e, f) 50°C with prolonged immersion time

Figure 4 shows the typical Nyquist and Bode plots for the corrosion of copper in the electrolyte of the Li-ions batteries for different exposure time at different temperatures. All impedance spectrum exhibit a similar characteristic, which consists of two indistinguishable depressed capacitive loops. The

capacitive loop in high frequency region is related to the corrosion product film on the copper, while the loop in low frequency region is related to the charge transfer resistance at the interface the electrolyte and copper.

At -20°C , the capacitive loops contract significantly from 3 h to 150 h and then keep stable. The contraction of the loops corresponds to an increasing corrosion rate of copper, as shown in Figure 4 a and b. Compared with the specimens corroded at -20°C , the total impedance of copper in the electrolyte at 25°C decreases approximately one order of magnitude, indicating an increasing corrosion rate. It is noted that the capacitive loops expanded significantly from 3 h to 24 h which also correlates to the formation of a protective film on the surface of the copper at the initial stage. This is consistent with the results that reported by Shu[21]. The capacitive loops decreased gradually until a 720 h immersion in the electrolyte.

As shown in Figure 4 e, the capacitive loops contract significantly after the copper corroded for 360 h in the electrolyte at 50°C . The impedance decreases about one order of magnitude compared with that corroded in the electrolyte at 25°C . Moreover, it could be observed that the rubber sealing cover of container was expanded after immersion about 480 h. This may correlate with the emission of the gas for the decomposition of the electrolyte at an elevated temperature[25].

The impedance behavior could be described by the equivalent circuit shown in Figure 5. In this equivalent circuit, R_s is the resistance of the electrolyte, Q_f is the capacitance of the corrosion product layer, and R_f represents the pore resistance of the corrosion product that forms on the surface of the copper. Additionally, R_t and Q_{dl} represent the charge transfer resistance and the double layer capacitance. In the fitting procedure, both C_f and C_{dl} were replaced with constant phase element (CPE) Q_f and Q_{dl} , respectively.

The complex impedance of the CPE can be defined by Equation 1[26-29]:

$$Z_{CPE} = \frac{1}{Y} (j\omega)^{-n} \quad (1)$$

where Y is the CPE, j is the imaginary unit (square = -1), ω is the angular frequency ($\omega = 2\pi f$, f is the frequency) of the AC voltage applied to the electrolyte cell, and n represents the deviation of the ideal capacitance behavior.

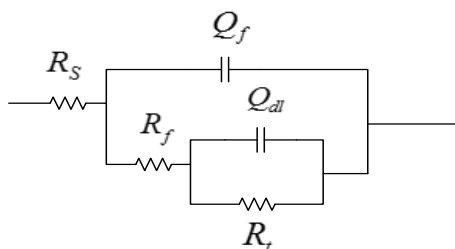


Figure 5. Equivalent circuit used to fit the EIS diagrams for copper in the electrolyte

Figure 6 shows the variation of the fitted values for R_f and R_t of copper versus time in the electrolyte at different temperatures. The value of R_f and R_t obtained from the impedance of copper

corroded at -20°C are significantly greater than those obtained at 25°C and 50°C . R_f and R_t of impedance spectroscopy for the corrosion of copper at -20°C and 25°C increase significantly after immersion for 24 h, indicating that a dense and protective film forms on the copper.

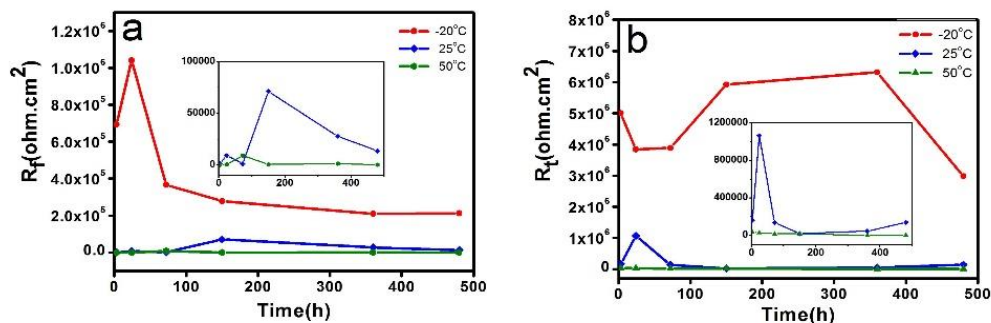


Figure 6. The fitted (a) R_f and (b) R_t at different temperatures for the corrosion of copper in the electrolyte

R_s refers to the solution resistance of the electrolyte. Scantlebury demonstrated that the resistance of the electrolyte solution (R_s) decreases uniformly as the solution conductance increased and its actual values agree well with the resistance calculated for the solutions[30]. The temperature influences the stability of the solution, as well as its conductivity. In this work, R_s is used to reflect the chemical stability and conductivity of the electrolyte at different temperatures. Figure 7 shows the variation of R_s obtained from EIS at -20°C , 25°C and 50°C for the total immersion time. It was observed that R_s at -20°C is much higher than the others, indicating an decreased solution conductivity. The pitting propagation rate is associated with the ohmic drop in potential between the cathodic and anodic reaction sites in situation.²³ The lower conductivity of electrolyte signifies the greater ohmic resistance, which retards the developments of pitting holes. Therefore, it could be observed that the pitting corrosion on the surface of copper at -20°C is slighter than that at 25°C , as shown in Figure 1.

R_s obtained at 25°C almost stays constant at approximately 75 ohm.cm^2 until a 720 h-immersion, which indicates an excellent stability of the electrolyte at ambient temperatures. In contrast, R_s obtained from the electrolyte at 50°C increases gradually from 96 h until 480 h, which suggests that the composition alter at 50°C due to the decomposition of electrolyte. The visible expansion of the sealing rubber after immersion for 480 h also proves that a certain amount of gas was produced due to the decomposition of the electrolyte at an elevated temperature. Considering that there may exist a slight air leak, the experiments were halted after immersion for 480 h.

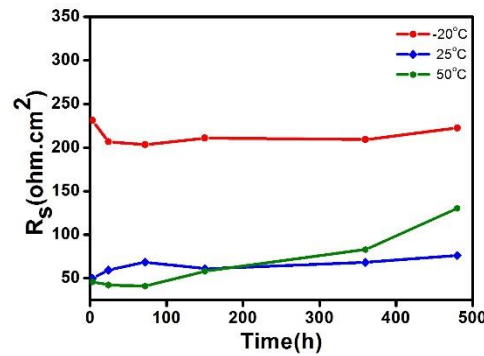


Figure 7. The fitted R_s at different temperatures for the corrosion of copper in the electrolyte

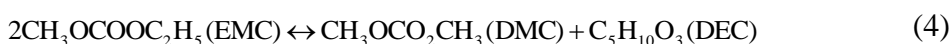
The trace amount of water in the nonaqueous electrolytes of LIBs has a significantly negative impact on the electrochemical performance of the batteries due to the reduction at the anode to generate H_2 and oxidation at cathode to release O_2 [31]. Besides that, the residual water has high reactivity with the commonly used $LiPF_6$ salt to produce HF in the electrolyte. The reactions are as follows[32]:



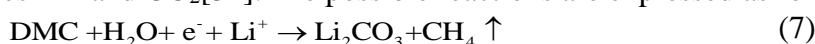
According to chemical thermodynamics, copper can hardly be corroded in the deoxygenated acid solution since copper cannot replace hydrogen from acid solutions. However, in this work, copper could be oxidized by the trace amount of water in the organic electrolyte of a lithium ion battery with the formation of CuO_x . Alternatively, HF reacts with CuO_x with the production of H_2O and CuF_2 .

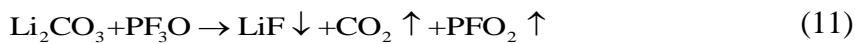
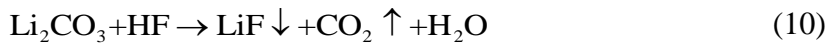
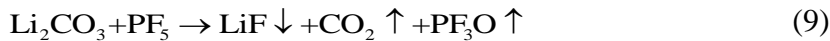
Subsequently, the generated water at the local attacked zone resumed reacting with the underlying bare copper. Simultaneously, it also promotes the decomposition of PF_5 around the defects and produce HF, which results in the further dissolution of copper oxides at the attacked zone. It can be assumed that the water at the local attacked zone causes the local corrosion as self-catalyst and facilitate the pit propagation. Thus, obvious pitting holes could be observed on the copper that was corroded at $-20^\circ C$ and $25^\circ C$ in the electrolyte for 480h.

In contrast, a thick layer is observed on the surface of copper and no pitting holes are not observed on the samples that corroded in the electrolyte at $50^\circ C$. The obvious variation of solution resistance during the total immersion time and the gas release proves that the electrolyte decompose spontaneously at an elevated temperature. The relevant reactions are as follows[25,33]:



Simultaneously, Li^+ in the batteries could react with DEC and DMC, forming compounds containing Li_2CO_3 . Li_2CO_3 subsequently reacts with PF_5 or HF stemming from the hydrolysis of PF_5 and generates LiF and CO_2 [34]. The possible reactions are expressed as follows[35-36]:





The above-mentioned reactions could explain that a loose layer that contains a certain amount of LiF forms on the surface of the specimens at 50°C and some gas released after 480 h immersion in the electrolyte. As shown in Eq.(7), water reacts with DMC and Li⁺ and produces Li₂CO₃, which restrains the oxidation of copper by the residual water in the electrolyte. Meanwhile, the consumption of fluorine element on the surface of copper, as shown in Eq.(9)-(11), also depresses the local corrosion of copper. These reactions could explain that no obvious pitting holes are observed on the copper that exposed to the electrolyte at 50°C.

4. CONCLUSIONS

In this paper, the corrosion performance of copper foil collectors in lithium ion battery electrolytes at -20°C, 25°C and 50°C were studied by electrochemical method. Corrosion pits can be observed on the surface of copper corroded in the electrolyte at -20°C and 25°C. No pitting holes were observed when copper corrodes in the electrolyte at 50°C and a thick layer containing a certain amount of LiF formed on the specimens. Corrosion current density of copper immersed in the electrolyte enhances with the increase of temperature, indicating an increasing corrosion rate. EIS results shows that the solution resistance at -20°C is significantly higher than that at 25°C. The decomposition of the electrolyte at 50°C contributes to the increase of electrolyte resistance with an extension of the immersion time. The self-catalyst effects of water at the local zone promotes the pit propagation, which results in the formation of pitting holes on the samples corroded at -20°C and 25°C. The exhaustion of water and fluorine ions during the decomposition of electrolyte were inclined to depress the local corrosion of copper that exposed to the electrolyte at 50°C.

ACKNOWLEDGMENTS

This work was supported by the National Natural Science Foundation of China (No.51471036 and No.51771034).

References

1. M. Armand, D. Murphy and J. Broadhead, *Materials for Advanced Batteries*[M]. New York: Plenum Press, 1980: 145.
2. A. Reyes Jiménez, R. Klöpsch, R. Wagner, U.C. Rodehorst, M. Kolek, R. Nölle, M. Winter and T. Placke, *ACS Nano.*, 11 (2017) 4731.
3. B. Liang, Y.P. Liu and Y.H. Xu, *J. Power Sources*, 267 (2014) 469.
4. X. Wang, H.M. Hua, L.Q. Peng, B.Y. Huang and P. Zhang, *Appl. Surf. Sci.*, 542 (2021) 148661.
5. Y.F. Li, Q.H. Li and Z.C. Tan, *J. Power Sources*, 443 (2019) 227262.
6. M. Armand and J.M. Tarascon, *Nature*, 451 (2008) 652.

7. J.M. Tarascon and M. Armand, *Nature.*, 414 (2001) 359.
8. M.T.F. Rodrigues, G. Babu, H. Gullapalli, K. Kalaga, F.N. Sayed, K. Kato, J. Joyner and P.M. Ajayan, *Nat. Energy.*, 2 (2017) 17108.
9. H.M. Cho, W.S. Choi, J.Y. Go, S.E. Bae and H.C. Shin, *J. Power Sources*, 198 (2012) 273.
10. T.R. Jow, J.L. Allen, B. Deveney and K. Nechev, *Ecs. Transactions.*, 16 (2009) 163.
11. X. Kang, *J. Electrochem. Soc.*, 154 (2007) A162.
12. M.C. Smart, B.V. Ratnakumar, L. Whitcanack, K. Chin, M. Rodriguez and S. Surampudi, *IEEE Aero El Sys Mag.*, 17 (2002) 16.
13. M.C. Smart, B.V. Ratnakumar, A. Beha, L.D. Whitcanack, J.S. Yu and M. Alamgir, *J. Power Sources*, 165 (2007) 535.
14. C.K. Huang, J.S. Sakamoto, J. Wolfenstine and S. Surampudi, *J. Electrochem Soc.*, 147 (2000) 2893.
15. C.F. Chen, P. Barai and P.P. Mukherjee, *J. Electrochem. Soc.*, 161 (2014) A2138.
16. H.L. Zou, H.F. Xiang, X. Liang, X.Y. Feng, S. Cheng, Y. Jin and C.H. Chen, *J. Alloys Compd.*, 701 (2017) 99.
17. H. Yin, M.L. Cao, X.X. Yu, C. Li, Y. Shen and M.Q. Zhu, *Rsc Adv.*, 7 (2017) 13250.
18. S. Yang, H. Qin, X. Li, H. Li and P. Yao, *J. Nanomater.*, 2017 (2017) 6948183.
19. S.S. Zhang, K. Xu and T.R. Jow, *Electrochem. Commun.*, 4 (2002) 928.
20. X. Zhang, B. Winget, M. Doeff, J.W. Evans and T.M. Devine, *J. Electrochem Soc.*, 152 (2005) 1310.
21. J. Shu, M. Shui, F. Huang, D. Xu, Y. Ren, L. Hou, J. Cui and J. Xu, *Electrochim. Acta*, 56 (2011) 3006.
22. S.W. Dai, J. Chen, Y.J. Ren, Z.M. Liu, J.L. Chen, C. Li, X.Y. Zhang, X. Zhang and T.F. Zeng, *Int. J. Electrochemical Sci.*, 12 (2017) 10589.
23. J. Soltis, *Corros. Sci.*, 90 (2015) 5.
24. S. Hejazi, S. Mohajernia, M.H. Moayed, A. Davoodi, M. Rahimizadeh, M. Momeni, A. Eslami, A. Shiri and A. Kosari, *J. Ind. Eng. Chem.*, 25 (2014) 112.
25. Q. Wang, J. Sun and C. Chen, *Rare Metals*, 25 (2006) 94.
26. P. Mishra, D. Yavas, A.F. Bastawros and K.R. Hebert, *Electrochim. Acta*, 346 (2020) 136232.
27. Y.J. Ren, J. Chen, C.L. Zeng, C. Li and J.J. He, *Int. J. Hydrogen Energ.*, 41 (2016) 8542.
28. S. Al-Saadi, P.C. Banerjee and R.K. Singh Raman, *Prog. Org. Coat.*, 111 (2017) 231.
29. K. Taweessup, P. Visuttiptikul, N. Yongvanich and G. Lothongkum, *Surf. Coat. Tech.*, 358 (2019) 732.
30. T.P. Hoar and W.R. Jacob, *Nature*, 216 (1967) 1299.
31. J.F. Qian, W. Xu, P. Bhattacharya, M. Engelhard, W.A. Henderson, Y.H. Zhang and J.G. Zhang, *Nano Energy*, 15 (2015) 135.
32. X.Z. Yu and H.H. Zheng, *J. Power Sources*, 24 (2002) 171.
33. G.G. Botte, R.E. White and Z. Zhang, *J. Power Sources*, 97 (2001) 570.
34. G. Ning, B. Haran and B.N. Popov, *J. Power Sources*, 117 (2003) 160.
35. Q. Wang, J. Sun, X. Yao and C. Chen, *Thermochim. Acta*, 437 (2005) 12.
36. O. Haik, F.S. Amalraj, D. Hirshberg, L. Burlaka, M. Talianker, B. Markovsky, E. Zinigrad, D. Aurbach, J.K. Lampert, J.Y. Shin, M. Schulz-Dobrick and A. Garsuch, *J. Solid State Electr.*, 18 (2014) 2333.